Original Article | Genitourinary Imaging

https://doi.org/10.3348/kjr.2016.17.6.853
pISSN 1229-6929 · eISSN 2005-8330
Korean J Radiol 2016;17(6):853-863

Korean Journal of Radiology
KJR

Comparison of Biexponential and Monoexponential Model of Diffusion-Weighted Imaging for Distinguishing between Common Renal Cell Carcinoma and Fat Poor Angiomyolipoma

Yuqin Ding, MD[1], Mengsu Zeng, MD, PhD[1], Shengxiang Rao, MD[1], Caizhong Chen, MD[1], Caixia Fu, MD[2], Jianjun Zhou, MD[1]

[1]Department of Radiology, Zhongshan Hospital, Fudan University, Shanghai Institute of Medical Imaging, Shanghai 200032, China; [2]Siemens Shenzhen Magnetic Resonance Ltd., Shenzhen 518057, China

Objective: To compare the diagnostic accuracy of intravoxel incoherent motion (IVIM)-derived parameters and apparent diffusion coefficient (ADC) in distinguishing between renal cell carcinoma (RCC) and fat poor angiomyolipoma (AML).

Materials and Methods: Eighty-three patients with pathologically confirmed renal tumors were included in the study. All patients underwent renal 1.5T MRI, including IVIM protocol with 8 b values (0–800 s/mm^2). The ADC, diffusion coefficient (D), pseudodiffusion coefficient (D*), and perfusion fraction (f) were calculated. One-way ANOVA was used for comparing ADC and IVIM-derived parameters among clear cell RCC (ccRCC), non-ccRCC and fat poor AML. The diagnostic performance of these parameters was evaluated by using receiver operating characteristic (ROC) analysis.

Results: The ADC were significantly greater in ccRCCs than that of non-ccRCCs and fat poor AMLs (each $p < 0.010$, respectively). The D and D* among the three groups were significantly different (all $p < 0.050$). The f of non-ccRCCs were less than that of ccRCCs and fat poor AMLs (each $p < 0.050$, respectively). In ROC analysis, ADC and D showed similar area under the ROC curve (AUC) values (AUC = 0.955 and 0.964, respectively, $p = 0.589$) in distinguishing between ccRCCs and fat poor AMLs. The combination of D > 0.97 x 10^{-3} mm^2/s, D* < 28.03 x 10^{-3} mm^2/s, and f < 13.61% maximized the diagnostic sensitivity for distinguishing non-ccRCCs from fat poor AMLs. The final estimates of AUC (95% confidence interval), sensitivity, specificity, positive predictive value, negative predictive value and accuracy for the entire cohort were 0.875 (0.719–0.962), 100% (23/23), 75% (9/12), 88.5% (23/26), 100% (9/9), and 91.4% (32/35), respectively.

Conclusion: The ADC and D showed similar diagnostic accuracy in distinguishing between ccRCCs and fat poor AMLs. The IVIM-derived parameters were better than ADC in discriminating non-ccRCCs from fat poor AMLs.

Keywords: *Intravoxel incoherent motion; Diffusion-weighted imaging; DWI; Renal cell carcinoma; Angiomyolipoma*

INTRODUCTION

Renal cell carcinoma (RCC) is the most common malignant renal tumor in adults, with three major subtypes including clear cell RCC (ccRCC), papillary RCC (pRCC), and chromophobe RCC (chRCC), accounting for 70–80%, 14–17%, and 4–8% of all RCCs, respectively (1). The number of detected renal tumors has been rising, possibly due to increased utilization of cross-sectional imaging (2, 3). However, preoperative characterization of benign and malignant renal masses is imperfect, and approximately 2–6% of the benign solid masses excised from the kidney in surgical series are angiomyolipomas (AML) (4-6). Most renal AMLs are diagnosed by detecting macroscopic fat on computed tomography (CT) or magnetic resonance imaging (MRI) (7). However, about 5–8% of AMLs with below

Received October 31, 2015; accepted after revision June 26, 2016.
Corresponding author: Jianjun Zhou, MD, Department of Radiology, Zhongshan Hospital, Shanghai Institute of Medical Imaging, 180 Fenglin Road, Shanghai 200032, China.
• Tel: (86) 13661497109 • Fax: (8621) 64439906
• E-mail: zhoujianjunzs@126.com

detectable fat levels on radiological study are referred to as fat poor AMLs (8). Differentiation among ccRCC, non-ccRCC and fat poor AML is difficult but essential for treatment planning (9, 10).

Contrast-enhanced CT and conventional MRI are routinely used in the evaluation of renal lesions. However, the use of contrast materials is contraindicated in some patients with renal functional impairment, as a result, unenhanced imaging techniques are of particular help in evaluating such patients. Diffusion-weighted imaging (DWI) derives image contrast from differences in the mobility (Brownian motion) of water in tissues without contrast administration. The degree of diffusion restriction of water molecules in tissue is quantified with apparent diffusion coefficient (ADC) in units of mm^2/s. DWI is increasingly used in the evaluation of benign and malignant renal lesions. Renal tumors show significantly lower ADC values, as compared with benign renal lesions (11-14). However, the reported ADC values of fat poor AML shows a non-negligible overlap with that of malignant renal lesions (15-17). In addition, contrasting results of ADC in different RCC subtypes are reported in the literature, and quantitative measurements from earlier monoexponential studies on renal masses are hardly comparable.

In 1986, Le Bihan et al. (18) proposed the principles of intravoxel incoherent motion (IVIM) and suggested that using a more sophisticated approach to describe the relationship between signal attenuation in tissues with increasing b values would enable the estimation of quantitative parameters that separately reflect tissue diffusivity and microcapillary perfusion. Previous study has shown that IVIM-DWI is more accurate than monoexponential model of DWI in discriminating enhancing and non-enhancing renal lesions (19). In addition, IVIM-DWI is helpful for distinguishing between common RCC subtypes (20, 21). However, to the best of our knowledge, few studies focus on the value of IVIM-DWI for distinguishing between ccRCC, non-ccRCC and fat poor AML. Therefore, the purpose of our study was to compare the diagnostic accuracy of IVIM-derived parameters and ADC for distinguishing between common RCC and fat poor AML.

MATERIALS AND METHODS

Patients

Our Institutional Review Board waived the requirement of informed patient consent and approved this retrospective study protocol. One hundred and twenty-two patients who presented to our department with known or suspected history of renal neoplasms between May 2013 and August 2015, were included in the study. Sixteen patients were excluded on pathologic analysis due to renal neoplasms other than ccRCC, pRCC, or chRCC, including multilocular cystic RCC (n = 3), liposarcoma (n = 1), non-Hodgkin lymphoma (n = 1), clear cell papillary RCC (n = 1), Xp11.2 translocation/TFE3 gene fusion associated RCC (n = 1), unclassified RCC (n = 1), transitional cell tumor (n = 5), metanephric adenoma (n = 1), oncocytoma (n = 1), and complex cyst (n = 1). In addition, three AMLs with bulk fat were also excluded. Furthermore, patients with enhancing renal masses with lack of histopathologic correlation (n = 13), excessive motion-induced image artifacts (n = 4), and tumors < 1 cm in diameter (n = 3) were also excluded. The final study population included 83 patients with 48 ccRCCs, 11 pRCCs, 12 chRCCs, and 12 fat poor AMLs. For 4 patients with > 1 RCCs, only the largest lesion was chosen for further analysis. Fat poor AMLs in our study referred to renal masses with pathologic confirmed AML and without visible fat in cross-sectional imaging (routine MRI protocols especially the transverse T1-weighted dual-echo in-phase and out-of-phase sequences, slice thickness 3–5 mm).

Routine MRI Protocols

MRI examinations were performed with a 1.5T MRI system (Magnetom Aera; Siemens Healthcare, Erlangen, Germany). Patients were imaged in supine position by

Table 1. Characteristics of Patients and Renal Lesions

Characteristic	All Lesions	ccRCC	Non-ccRCC	Fat poor AML
Number of lesions	83	48	23	12
Size, mean ± SD (range), cm	3.7 ± 2.0 (1.2–14.5)	3.8 ± 1.3 (1.8–6.7)	3.6 ± 2.8 (1.2–14.5)	3.4 ± 2.6 (1.8–11.2)
Age, mean ± SD (range), year	52 ± 12 (28–75)	55 ± 11 (31–75)	52 ± 11 (35–67)	44 ± 13 (28–71)
Sex, female/male	35/48	15/33	10/13	10/2
Side, left/right	41/42	23/25	10/13	8/4
Surgery, partial/radical	40/43	17/31	12/11	11/1

AML = angiomyolipoma, ccRCC = clear cell RCC, non-ccRCC = papillary RCC and chromophobe RCC, RCC= renal cell carcinoma

Korean Journal of Radiology
KJR

using an 18-channel body phase array coil as receiver. For morphologic evaluation of the kidneys, transverse fat-suppressed fast spin echo (TSE) T2-weighted imaging were initially performed, followed by transverse T1-weighted dual-echo in-phase and out-of-phase sequences and by transverse 3-dimensional fat-suppressed gradient echo (volume interpolated breath-hold examination) precontrast and postcontrast T1-weighted sequences under suspended respiration.

Table 2. ADC and IVIM-Derived Parameters of Renal Lesions on Basis of Histologic Subtypes

Parameters	ccRCC	Non-ccRCC	Fat poor AML
ADC (10^{-3} mm^2/s)	1.71 ± 0.32	1.23 ± 0.32	1.10 ± 0.21
D (10^{-3} mm^2/s)	1.42 ± 0.35	1.04 ± 0.27	0.80 ± 0.13
D* (10^{-3} mm^2/s)	26.75 ± 10.33	19.78 ± 8.99	34.66 ± 14.17
f (100%)	22.25 ± 6.52	13.96 ± 6.10	22.63 ± 7.73

Data were means ± standard deviation. AML = angiomyolipoma, ccRCC = clear cell RCC, non-ccRCC = papillary RCC and chromophobe RCC, RCC = renal cell carcinoma

IVIM-DWI

Transverse free-breathing twice-refocused spin echo, bipolar gradient, single-shot echo planar IVIM-DWI, with tridirectional trace-weighting diffusion gradients, was performed before contrast administration, using a work-in-progress echo planar imaging sequence (WIP NO. 870) provided by the manufacturer (Siemens Healthcare, Erlangen, Germany). This WIP package supports a motion insensitive PAT reference scan that is suitable for body diffusion measurements in free breathing mode. Sequence parameters for IVIM-DWI were as follows: FATSAT scheme, SPAIR; iPAT factor, 2; iPAT reference mode, flash; 8 b values (0, 25, 50, 80, 150, 300, 500, and 800 s/mm^2); averages 2; repetition time/echo time, 5100/70 ms; matrix, 128 x 128;

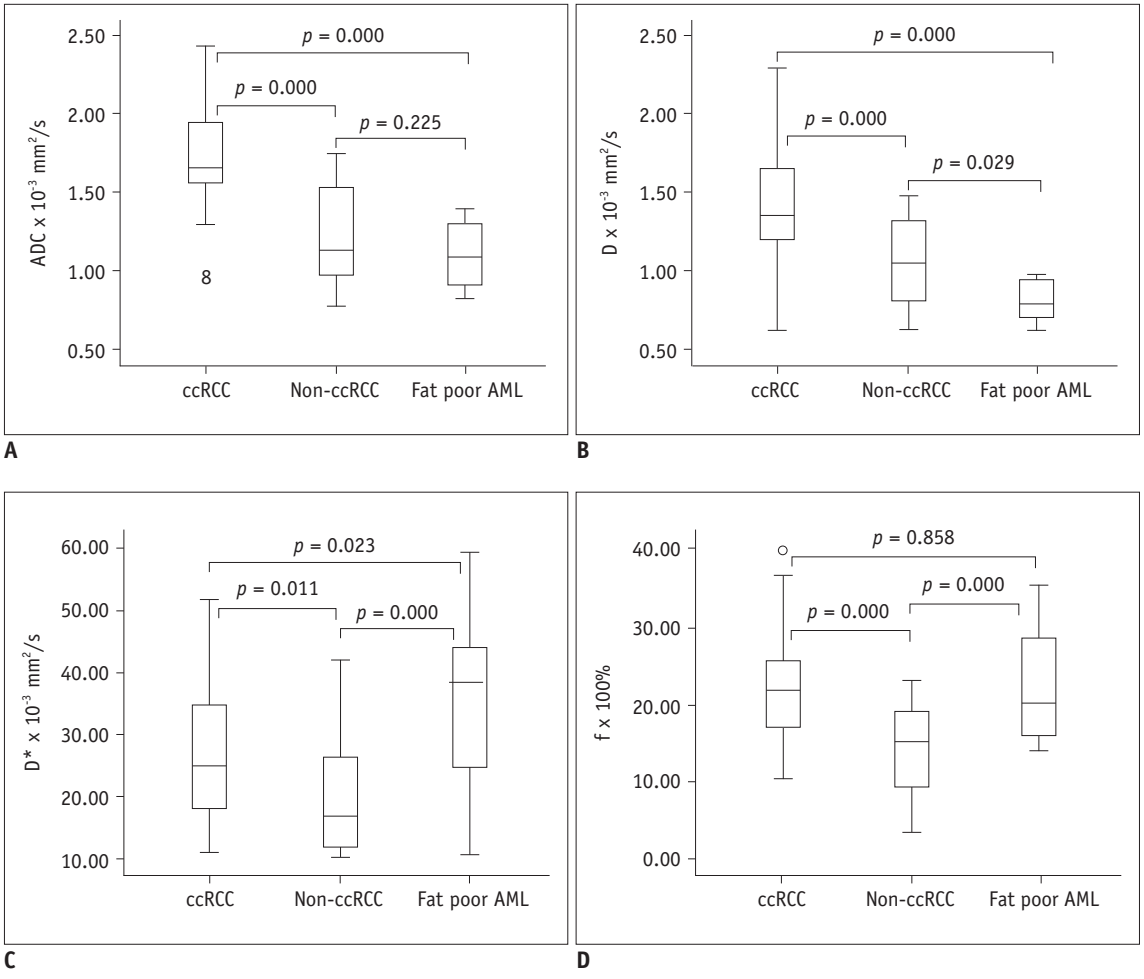

Fig. 1. Box-and-whisker plots of ADC (A), D (B), D* (C), and f (D) values for ccRCC, non-ccRCC, and fat poor AML. Bottom and top of boxes indicate 25th and 75th percentiles of values, respectively. Horizontal line inside box indicates median values. ADC = apparent diffusion coefficient, AML = angiomyolipomas, ccRCC = clear cell renal cell carcinoma, non-ccRCC = papillary RCC and chromophobe RCC

voxel size, 3.0 x 3.0 x 5.0 mm^3; bandwidth, 1698 Hz/pix; slice thickness, 5 mm; total acquisition time, 5 minutes 42 seconds.

MRI Analysis

Intravoxel incoherent motion-derived parameter maps (D, D*, f) were generated offline using the postprocessing program provided with WIP NO. 870 and fitting the following biexponential model (22): $S_b/S_0 = (1 - f).exp(-bD) + f.exp(-b[D^* + D])$, where S_b was the signal intensity at a given b value, S_0 was the signal intensity for b = 0 s/mm^2, f was the perfusion fraction of the diffusion linked to microcirculation, D was the diffusion parameter representing pure molecular diffusion, and D* was the pseudodiffusion coefficient representing incoherent microcirculation within the voxel. The fitting algorithm used in the postprocessing program was the same as described by Luciani et al. (22): initial estimation of D using a reduced set of b values larger than a predetermined value (200 s/mm^2) and subsequently, the resulting D as a fix parameter to fit the missing parameters.

Apparent diffusion coefficient was calculated with monoexponential fit of signal intensity using b = 0 and 800 s/mm^2 according to the following equation (22): $\ln(S_b) = \ln(S_0) - bADC$, where S_b is the signal intensity for each b value and S_0 is the signal intensity at a b value of zero.

All image measurements (D, D*, f, and ADC) were performed on the Syngo workstation (Siemens Healthcare, Erlangen, Germany). Identification of renal lesions and selection of the representative section for region of interest (ROI) placement were performed by two radiologists (with 4 and 18 years of experience in interpreting renal MR images, respectively) blinded to the clinical and pathologic information. A freehand ROI was drawn on the enhancing solid portion of the renal lesions on D map and the same ROI was copied to the D*, f, and ADC maps at the same level automatically, on the section containing the largest tumor cross-sectional area, excluding areas of hemorrhage and necrosis by comparing with T2-weighted and dynamic contrast-enhanced T1-weighted images. All ROI placements were decided by the two readers, independently. The ADC and IVIM-derived parameters for each reader were analyzed

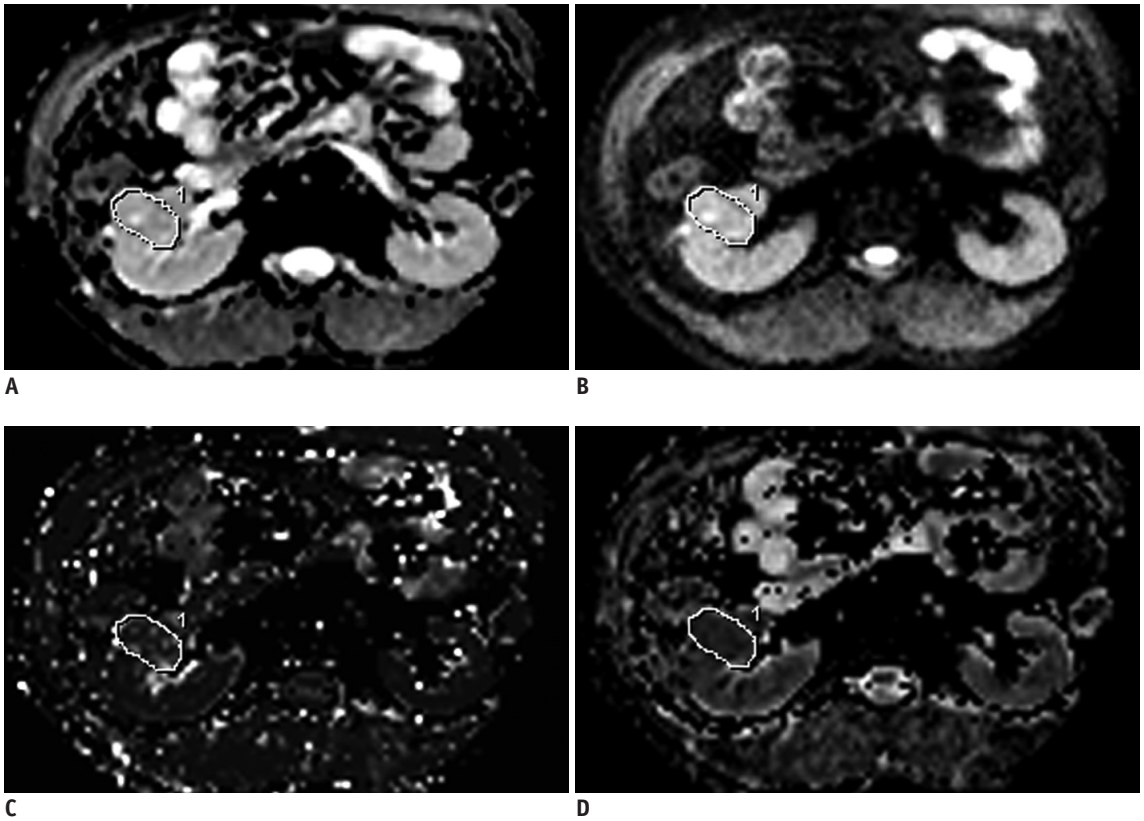

Fig. 2. MR images in 37-year-old man with 3.7 cm surgically verified ccRCC in right kidney.
Diffusion-weighted image with b value of 800 s/mm^2 **(A)**, and IVIM-derived parametric maps (D, D*, and f, respectively) **(B-D)** calculated from IVIM-DWI data. Calculated mean values of ADC, D, D*, and f for manually drawn ROIs for ccRCC were 1.85 x 10^{-3} mm^2/s, 1.49 x 10^{-3} mm^2/s, 31.10 x 10^{-3} mm^2/s, and 22.9%, respectively. ADC = apparent diffusion coefficient, ccRCC = clear cell renal cell carcinoma, DWI = diffusion-weighted imaging, IVIM = intravoxel incoherent motion, MR = magnetic resonance, ROIs = region of interests

Korean Journal of Radiology
KJR

by using the interclass correlation coefficient (ICC).

Statistical Analysis

The results from the more experienced reader (with 18 years of experience in interpreting renal MR images) were used for the main study analysis. Descriptive statistics were calculated for ADC and IVIM-derived parameters, and expressed as mean ± standard deviation (SD). One-way ANOVA was used to compare the differences of these parameters among ccRCCs, non-ccRCCs and fat poor AMLs. The least significant difference analysis was used for pairwise comparison. Receiver operating characteristic (ROC) curves were generated to evaluate the diagnostic performance of ADC and IVIM-derived parameters in differentiating ccRCCs and non-ccRCCs from fat poor AMLs. The sensitivity, specificity, positive predictive value (PPV), negative predictive value (NPV), accuracy, cut-off value, area under the ROC curve (AUC) as well as differences of AUCs were analyzed according to the method described by DeLong et al. (23). The optimal cut-off values of ADC and IVIM-derived parameters were calculated by using ROC curve analysis to achieve the highest Youden index. The AUC, sensitivity, specificity, PPV, NPV and accuracy for differentiating non-ccRCCs from fat poor AMLs were calculated using odds ratio (OR) combinations of the cutoff values of IVIM-derived parameters to maximize diagnostic accuracy (e.g., $D > 0.97 \times 10^{-3}$ mm^2/s or $D^* \leq 28.03 \times 10^{-3}$ mm^2/s or $f \leq 13.61\%$). Interobserver reliability of ADC and IVIM-derived parameters measurements was assessed by using ICCs. An *r* value of 1.0 was considered as perfect agreement; 0.81–0.99, almost perfect agreement; 0.61–0.80, substantial agreement; 0.41–0.60, moderate agreement; 0.21–0.40, fair agreement; and ≤ 0.20, slight agreement (24). All statistical analyses were performed using SPSS (version 19.0, IBM, Chicago, IL, USA) and MedCalc for Windows (version 14.8.1, Ostend, Belgium). Differences with *p* values of < 0.050 were considered significant.

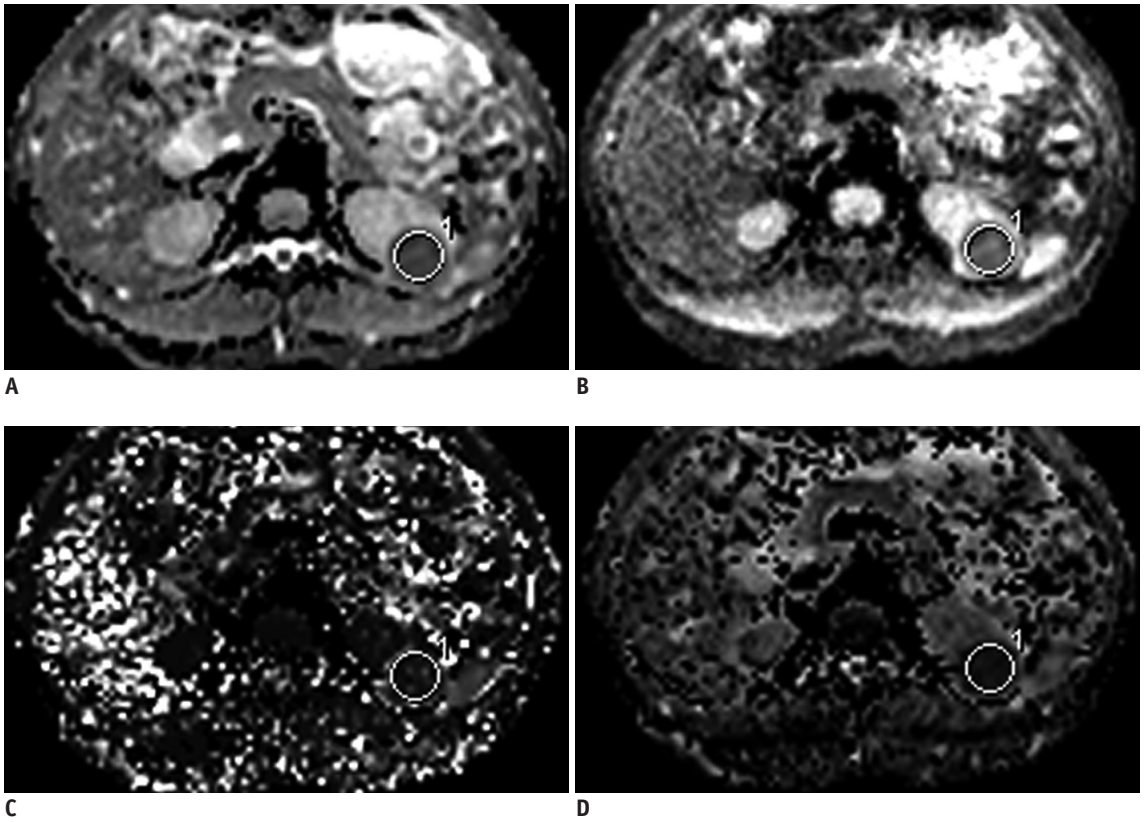

Fig. 3. MR images in 52-year-old man with 3.5 cm surgically proven chRCC in left kidney.
Diffusion-weighted image with b value of 800 s/mm^2 **(A)**, and IVIM-derived parametric maps (D, D*, and f, respectively) **(B-D)** calculated from IVIM-DWI data. Calculated mean values of ADC, D, D*, and f for manually drawn ROIs for non-ccRCC were 0.92×10^{-3} mm^2/s, 0.74×10^{-3} mm^2/s, 16.87×10^{-3} mm^2/s, and 13.9%, respectively. ADC = apparent diffusion coefficient, chRCC = chromophobe renal cell carcinoma, DWI = diffusion-weighted imaging, IVIM = intravoxel incoherent motion, MR = magnetic resonance, ROIs = region of interests

RESULTS

Lesion Characteristics

Of the 83 renal lesions included in this study, 48 (57.8%) were ccRCCs, 23 (27.7%) were non-ccRCCs, and 12 (14.5%) were fat poor AMLs. Baseline characteristics for each group were presented in Table 1. The patients comprised 48 men and 35 women (mean age 52 ± 12 years, range, 28–75 years). Patients with RCCs were predominantly male and older than that of fat poor AMLs (p = 0.010 and 0.002, respectively). Mean tumor sizes of RCCs and fat poor AMLs were not significantly different (3.8 ± 1.9 cm vs. 3.4 ± 2.6 cm, p = 0.583). Histopathologic analysis was performed on specimens acquired at radical (n = 43) or partial (n = 40) nephrectomy. Fat poor AMLs were surgically resected either because of failing to differentiate from malignant renal lesions (n = 8) or because of large tumor size (n = 4). The mean interval between MR examination and surgery was 8.4 ± 12.1 days (range, 0–72 days).

ADC and IVIM-Derived Parameters

Mean values ± SD of ADC and IVIM-derived parameters of ccRCCs, non-ccRCCs, and fat poor AMLs were described in Table 2. The ADC values were significantly greater in ccRCCs than that of non-ccRCCs and fat poor AMLs (both p < 0.010, respectively). However, ADC values of non-ccRCCs and fat poor AMLs were not significantly different (p = 0.225). The D and D* values among the three groups were significantly different (all p < 0.050), with the highest D values in ccRCCs and D* values in fat poor AMLs. The f values of non-ccRCCs were less than that of ccRCCs and fat poor AMLs (each p < 0.050, respectively). However, they were not significantly different between ccRCCs and fat poor AMLs (p = 0.858). Box-and-whisker plots of ADC and IVIM-derived parameters were displayed in Figure 1. Example maps of ADC and IVIM-derived parameters of the three groups were shown in Figures 2-4.

ROC Analysis

Receiver operating characteristic analysis of ADC and

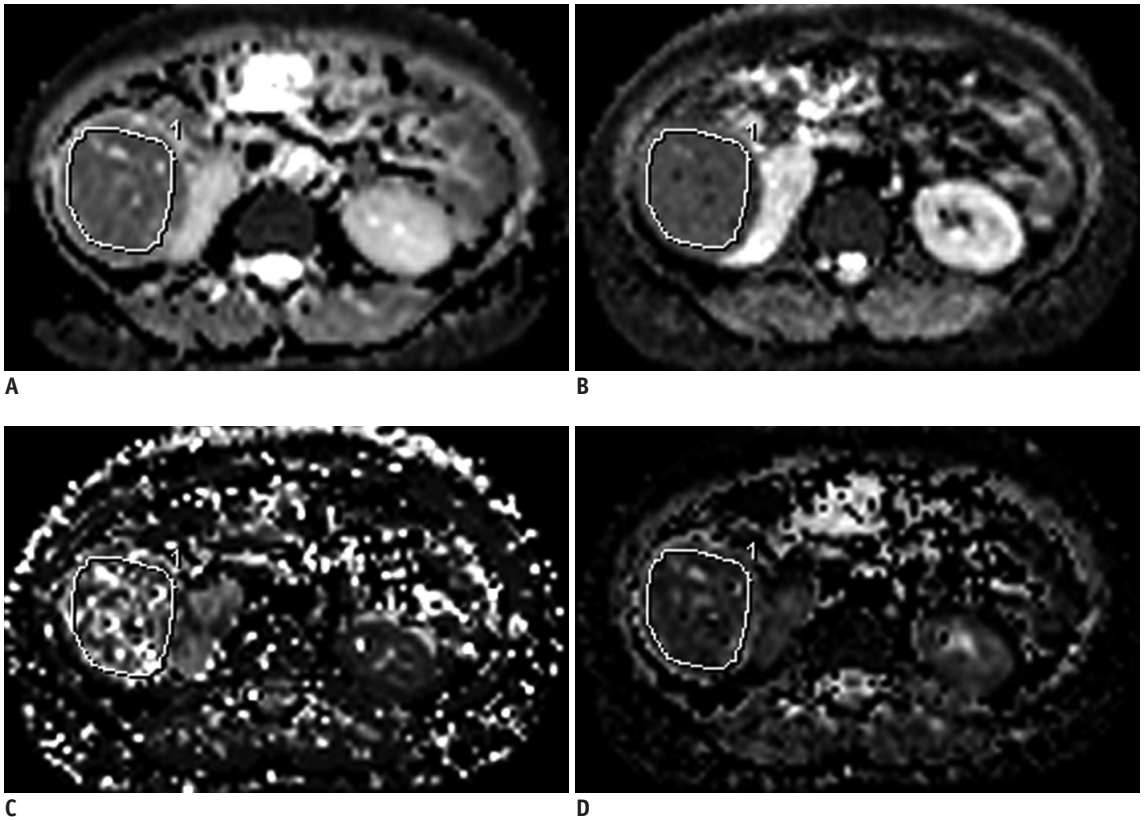

Fig. 4. MR images in 36-year-old woman with 11.2 cm pathologically proven fat poor AML in right kidney.
Diffusion-weighted image with b value of 800 s/mm^2 **(A)**, and IVIM-derived parametric maps (D, D*, and f, respectively) **(B-D)** calculated from IVIM-DWI data. Calculated mean values of ADC, D, D*, and f for manually drawn ROIs for fat poor AML were 1.16 x 10^{-3} mm^2/s, 0.81 x 10^{-3} mm^2/s, 50.55 x 10^{-3} mm^2/s, and 22.8%, respectively. ADC = apparent diffusion coefficient, AML = angiomyolipomas, DWI = diffusion-weighted imaging, IVIM = intravoxel incoherent motion, MR = magnetic resonance, ROIs = region of interests

Korean Journal of Radiology
KJR

Table 3. Results of ROC Analysis for ADC and IVIM-Derived Parameters in Differentiation between RCCs and Fat Poor AMLs

Comparison	AUC (95% CI*)	Sensitivity	Specificity	PPV	NPV	ACC	Cut-Off Value	*P*
ccRCC (n = 48) vs. fat poor AML (n = 12)								
ADC	0.955 (0.868–0.992)	85.4% (41/48)	100% (12/12)	100% (41/41)	63.2% (12/19)	88.3% (53/60)	> 1.39	< 0.001
D	0.964 (0.880–0.995)	93.8% (45/48)	100% (12/12)	100% (45/45)	80% (12/15)	95% (57/60)	> 0.97	< 0.001
D*	0.668 (0.535–0.785)	89.6% (43/48)	50% (6/12)	87.8% (43/49)	54.5% (6/11)	81.7% (49/60)	≤ 38.84	0.103
f	0.506 (0.374–0.638)	83.3% (40/48)	33.3% (4/12)	83.3% (40/48)	33.3% (4/12)	73.3% (44/60)	> 16.17	0.955
Non-ccRCC (n = 23) vs. fat poor AML (n = 12)								
ADC	0.634 (0.455–0.790)	39.1% (9/23)	100% (12/12)	100% (9/9)	46.2% (12/26)	60% (21/35)	> 1.39	0.167
D	0.757 (0.583–0.886)	56.5% (13/23)	100% (12/12)	100% (13/13)	54.5% (12/22)	71.4% (25/35)	> 0.97	0.002
D*	0.822 (0.656–0.930)	87% (20/23)	75% (9/12)	87% (20/23)	75% (9/12)	82.9% (29/35)	≤ 28.03	< 0.001
f	0.783 (0.611–0.904)	43.5% (10/23)	100% (12/12)	100% (10/10)	48% (12/25)	62.9% (22/35)	≤ 13.61	< 0.001

*Numbers in parentheses were 95% confidence intervals (CIs). ACC = accuracy, AML = angiomyolipoma, AUC = area under curve, ccRCC = clear cell RCC, non-ccRCC = papillary RCC and chromophobe RCC, NPV = negative predictive value, PPV = positive predictive value, RCC = renal cell carcinoma

IVIM-derived parameters in discriminating ccRCCs and non-ccRCCs from fat poor AMLs were summarized in Table 3 and Figure 5. In ROC analysis, ADC and D showed similar AUC values (AUC = 0.955 and 0.964, respectively, $p = 0.589$) in distinguishing between ccRCCs and fat poor AMLs. In the pairwise comparison of ROC curves among the parameters for differentiating ccRCCs from fat poor AMLs, ADC and D showed significantly greater AUC values than those of D* and f (all $p < 0.010$). The diagnostic accuracy of ADC, D, D*, and f for distinguishing ccRCCs from fat poor AMLs were 88.3% (53/60), 95% (57/60), 81.7% (49/60), and 73.3% (44/60), respectively. In addition, for distinguishing non-ccRCCs from fat poor AMLs, AUCs of IVIM-derived parameters were greater than that of ADC, without significance (all $p > 0.050$). The diagnostic accuracy of ADC, D, D*, and f for distinguishing non-ccRCCs from fat poor AMLs were 60% (21/35), 71.4% (25/35), 82.9% (29/35), and 62.9% (22/35), respectively. However, using the OR combination of D > 0.97 x 10^{-3} mm^2/s, D* < 28.03 x 10^{-3} mm^2/s and f < 13.61% maximized the diagnostic sensitivity. The final estimates of AUC (95% confidence interval [CI]), sensitivity, specificity, PPV, NPV, and accuracy for the entire cohort were 0.875 (0.719–0.962), 100% (23/23), 75% (9/12), 88.5% (23/26), 100% (9/9), and 91.4% (32/35), respectively.

Interobserver Agreement

Evaluation of the agreement between the two readers indicated that the ICCs (95% CI) for ADC and D were 0.911 (0.866–0.942) and 0.834 (0.754–0.889), respectively, indicating almost perfect agreement. The ICCs for D* and f were 0.748 (0.635–0.829) and 0.785 (0.686–0.855), respectively, indicating substantial agreement.

DISCUSSION

The present study compared the diagnostic accuracy of ADC and IVIM-derived parameters for distinguishing between common RCCs and fat poor AMLs. Our results demonstrated that ADC and D showed significantly greater AUC values (AUC = 0.955 and 0.964, respectively) than those of D* and f (AUC = 0.668 and 0.506, respectively, all $p < 0.010$). This might be due to the specific histological growth modality and tumor cellular density of ccRCCs and fat poor AMLs. The tumor cells of ccRCCs were often interspersed with cystic and hemorrhagic areas and separated by interstitial spaces so that water could spread

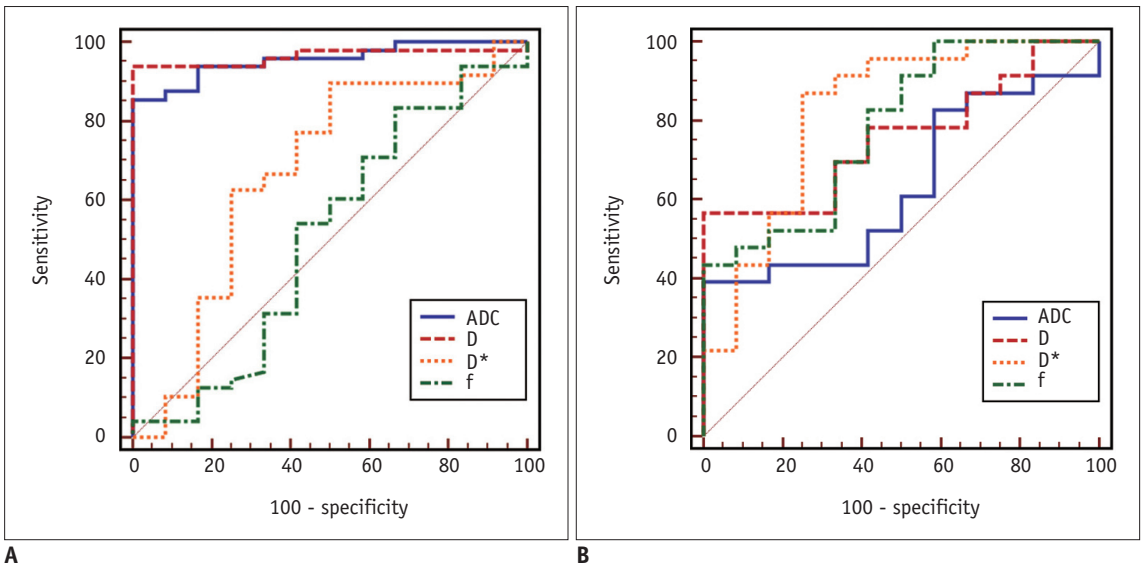

Fig. 5. ROC curves for ADC and IVIM-derived parameters in differentiating renal cell carcinomas and fat poor AMLs.
A. Graph shows comparison of ROC curve analysis for discriminating ccRCC and fat poor AMLs with ADC and IVIM-derived parameters. AUCs for ADC, D, D*, and f were 0.955, 0.964, 0.668, and 0.506, respectively. **B.** Graph shows comparison of ROC curve analysis for differentiation between non-ccRCC and fat poor AMLs with ADC and IVIM-derived parameters. AUCs for ADC, D, D*, and f were 0.634, 0.757, 0.822, and 0.783, respectively. ADC = apparent diffusion coefficient, AML = angiomyolipomas, AUC = area under the receiver operating characteristic curve, ccRCC = clear cell renal cell carcinoma, IVIM = intravoxel incoherent motion, ROC = receiver operating characteristic

freely (25). The greater cellular density and collagenous interstitial stroma that reduced water diffusion velocity might contribute to the decreased ADC and D values of fat poor AMLs (26, 27). In addition, both ccRCCs and fat poor AMLs were hypervascular renal lesions, and the increased D* and f values could be explained by vascular perfusion (10).

In our study, IVIM-derived parameters, especially the perfusion-related parameters (D* and f), showed greater diagnostic accuracy than that of ADC values in distinguishing non-ccRCCs from fat poor AMLs. In addition, using the OR combination of D > 0.97 x 10^{-3} mm^2/s, D* < 28.03 x 10^{-3} mm^2/s, and f < 13.6% maximized the diagnostic accuracy (91.4%, 32/35). However, the ADC values of non-ccRCCs and fat poor AMLs were not significantly different (p = 0.225). One possible reason might be that both non-ccRCCs and fat poor AMLs showed lower ADC values owing to compact tissue architecture and great cellular density (25, 26). Another possible reason might be that the ADC value was calculated by monoexponential fitting of diffusion decay data, containing both the perfusion and diffusion information. The variability of renal ADC values in healthy volunteers was analyzed in a previous study (27), the monoexponential fitting error was significantly higher than that of biexponential fittings, indicating that the monoexponential model was insufficient for renal tissues.

Although D* showed the greatest AUC value (AUC = 0.822) in differentiation between non-ccRCCs and fat poor AMLs in our study, paradoxical diagnostic value of D* was described in previous studies. Chandarana et al. (20) reported that the D* was not significantly different between different RCC subtypes. In addition, D* was not significantly different between enhancing masses and non-enhancing masses (p = 0.528) in another study (19). The promising diagnostic value of D* in our study might be due to our strict inclusion criteria for RCCs and fat poor AMLs, carefulness in ROI selection, and improved image quality with motion correction. Evaluation of the agreement between the two readers indicated that the ICCs for D* and f were 0.748 (0.635–0.829) and 0.785 (0.686–0.855), respectively, which indicated substantial agreement. However, artefacts from great vessels and cystic areas of the renal lesions on D* maps were still inevitable. As a result, efforts should be made to improve the image quality of D* maps in order to make this parameter more reliable and reproducible.

Previous studies demonstrated that IVIM-DWI could be used to derive both perfusion and diffusion parameters of renal lesions without contrast material. A study by Chandarana et al. (19) showed that the IVIM-derived parameters were more accurate than ADC in distinguishing between enhancing and non-enhancing renal lesions; they subsequently showed the usefulness of IVIM-DWI in distinguishing some RCC subtypes (20). In addition, the perfusion-related parameter (f value) correlated well with enhancement degree of renal lesions, accurately separating

Korean Journal of Radiology
KJR

avidly enhancing ccRCC and chRCC from hypoenhancing pRCC and cystic RCC. Furthermore, pRCC and cystic RCC could be further separated by degree of tumor cellularity as captured by the metric D, which was higher in cystic RCC, reflecting decreased cellularity in the predominantly cystic tumor. However, only 3 cases of AMLs were included in a study using voxel-based histogram analysis of IVIM-derived parameters (28). In our study, IVIM-derived parameters showed the possibility of simultaneously providing information about perfusion and diffusion characteristics of renal tumors and demonstrated greater diagnostic accuracy when compared with ADC in discriminating non-ccRCCs from fat poor AMLs.

Although the ADC value showed significant difference between benign and malignant renal lesions in some studies (13, 15-17), it was not possible to confidently distinguish fat poor AMLs from RCCs. This difficulty might arise from considerable variation and overlap between the ADC values of fat poor AMLs and malignant renal lesions. In common subtypes of RCCs, published ADC values varied from 1.23 x 10^{-3} mm^2/s to 2.11 x 10^{-3} mm^2/s in ccRCCs, 0.61 x 10^{-3} mm^2/s to 2.07 x 10^{-3} mm^2/sec in pRCCs, and 0.99 x 10^{-3} mm^2/s to 1.74 x 10^{-3} mm^2/s in chRCCs, respectively (13, 17, 26, 29-31). However, the reported ADC values of fat poor AMLs showed a significant overlap with that of malignant renal lesions, ranging from 0.72 x 10^{-3} mm^2/s to 1.11 x 10^{-3} mm^2/s (15-17). Several possible explanations exist for the wide range of ADC values of renal lesions, including errors, different methods of ADC measurements, different b values, and imaging protocols. A major challenge to the widespread implementation of DW-MRI is the lack of a standard approach to data collection and analysis (32).

The optimal b values for renal DWI have not yet been determined. In our study, b values of 0 and 800 s/mm^2 were selected based on the study by Wang et al. (33). In their study, compared with the ADC obtained by using b values of 0 and 500 s/mm^2, the ADC obtained by using b values of 0 and 800 s/mm^2 could better reflect the diffusion characteristics of common RCC subtypes. In addition, b values > 1000 s/mm^2 were not selected because of longer echo time, worse signal-to-noise ratio, and greater image distortion. Eight b values (ranged from 0 to 800 s/mm^2) were selected for IVIM model of DWI in our study according to the recommendations of Koh et al. (34), which suggested that 8 to 8 b values in total, with ≥ 4 within the perfusion-sensitive range (b < 100 s/mm^2) would be sufficient to evaluate perfusion-related parameters in the clinical setting.

This study had several limitations. Firstly, image misalignment due to respiratory motion might influence the reliability of our result because IVIM-DWI was acquired during free breathing. However, according to a recent study (35), free breathing was recommended for liver DWI because of its good reproducibility and shorter acquisition time, as compared with that of multi-breath hold, respiratory triggered, and navigator triggered techniques. DWI of the kidney should be less affected by respiratory motion due to its location, as compared with the liver. In addition, our WIP package (NO. 870) provided by the manufacturer supported a motion insensitive PAT reference scan that was suitable for body diffusion measurements in free breathing mode. As a result, image misalignment should not be a critical problem for our study. Secondly, there were a limited number of patients with non-ccRCCs and fat poor AMLs; therefore, we provided preliminary results by using a relatively small sample size, and further studies in larger populations are warranted. Thirdly, we did not analyze conventional MR protocols (T2-weighted imaging, multiple phase contrast enhanced imaging, etc.) and did not compare IVIM-derived perfusion related parameters (D* and f) with other techniques (arterial spin labeling, dynamic contrast enhanced MR imaging, etc.) in evaluation of vascularity of renal lesions. Therefore, additional studies are required to assess the incremental benefits of the IVIM-derived parameters in the evaluation of renal lesions, especially in patients with impaired renal function.

In conclusion, biexponential fit analysis of DWI could be used to explore the perfusion and diffusion characteristics of renal tumors. The ADC and D showed similar diagnostic accuracy in distinguishing between ccRCCs and fat poor AMLs. The combination of IVIM-derived parameters were better than ADC values in discriminating non-ccRCCs from fat poor AMLs.

REFERENCES

1. Kovacs G, Akhtar M, Beckwith BJ, Bugert P, Cooper CS, Delahunt B, et al. The Heidelberg classification of renal cell tumours. *J Pathol* 1997;183:131-133
2. Hollingsworth JM, Miller DC, Daignault S, Hollenbeck BK. Rising incidence of small renal masses: a need to reassess treatment effect. *J Natl Cancer Inst* 2006;98:1331-1334
3. Karaosmanoğlu AD, Onur MR, Shirkhoda A, Ozmen M, Hahn PF. Unusual malignant solid neoplasms of the kidney: cross-sectional imaging findings. *Korean J Radiol* 2015;16:853-859

4. Woo S, Cho JY. Imaging findings of common benign renal tumors in the era of small renal masses: differential diagnosis from small renal cell carcinoma: current status and future perspectives. *Korean J Radiol* 2015;16:99-113
5. Milner J, McNeil B, Alioto J, Proud K, Rubinas T, Picken M, et al. Fat poor renal angiomyolipoma: patient, computerized tomography and histological findings. *J Urol* 2006;176:905-909
6. Fujii Y, Komai Y, Saito K, Iimura Y, Yonese J, Kawakami S, et al. Incidence of benign pathologic lesions at partial nephrectomy for presumed RCC renal masses: Japanese dual-center experience with 176 consecutive patients. *Urology* 2008;72:598-602
7. Halpenny D, Snow A, McNeill G, Torreggiani WC. The radiological diagnosis and treatment of renal angiomyolipoma-current status. *Clin Radiol* 2010;65:99-108
8. Jinzaki M, Silverman SG, Akita H, Nagashima Y, Mikami S, Oya M. Renal angiomyolipoma: a radiological classification and update on recent developments in diagnosis and management. *Abdom Imaging* 2014;39:588-604
9. Catalano OA, Samir AE, Sahani DV, Hahn PF. Pixel distribution analysis: can it be used to distinguish clear cell carcinomas from angiomyolipomas with minimal fat? *Radiology* 2008;247:738-746
10. Hindman N, Ngo L, Genega EM, Melamed J, Wei J, Braza JM, et al. Angiomyolipoma with minimal fat: can it be differentiated from clear cell renal cell carcinoma by using standard MR techniques? *Radiology* 2012;265:468-477
11. Squillaci E, Manenti G, Di Stefano F, Miano R, Strigari L, Simonetti G. Diffusion-weighted MR imaging in the evaluation of renal tumours. *J Exp Clin Cancer Res* 2004;23:39-45
12. Cova M, Squillaci E, Stacul F, Manenti G, Gava S, Simonetti G, et al. Diffusion-weighted MRI in the evaluation of renal lesions: preliminary results. *Br J Radiol* 2004;77:851-857
13. Zhang J, Tehrani YM, Wang L, Ishill NM, Schwartz LH, Hricak H. Renal masses: characterization with diffusion-weighted MR imaging--a preliminary experience. *Radiology* 2008;247:458-464
14. Taouli B, Thakur RK, Mannelli L, Babb JS, Kim S, Hecht EM, et al. Renal lesions: characterization with diffusion-weighted imaging versus contrast-enhanced MR imaging. *Radiology* 2009;251:398-407
15. Tanaka H, Yoshida S, Fujii Y, Ishii C, Tanaka H, Koga F, et al. Diffusion-weighted magnetic resonance imaging in the differentiation of angiomyolipoma with minimal fat from clear cell renal cell carcinoma. *Int J Urol* 2011;18:727-730
16. Agnello F, Roy C, Bazille G, Galia M, Midiri M, Charles T, et al. Small solid renal masses: characterization by diffusion-weighted MRI at 3 T. *Clin Radiol* 2013;68:e301-e308
17. Sasamori H, Saiki M, Suyama J, Ohgiya Y, Hirose M, Gokan T. Utility of apparent diffusion coefficients in the evaluation of solid renal tumors at 3T. *Magn Reson Med Sci* 2014;13:89-95
18. Le Bihan D, Breton E, Lallemand D, Grenier P, Cabanis E, Laval-Jeantet M. MR imaging of intravoxel incoherent motions: application to diffusion and perfusion in neurologic disorders. *Radiology* 1986;161:401-407
19. Chandarana H, Lee VS, Hecht E, Taouli B, Sigmund EE. Comparison of biexponential and monoexponential model of diffusion weighted imaging in evaluation of renal lesions: preliminary experience. *Invest Radiol* 2011;46:285-291
20. Chandarana H, Kang SK, Wong S, Rusinek H, Zhang JL, Arizono S, et al. Diffusion-weighted intravoxel incoherent motion imaging of renal tumors with histopathologic correlation. *Invest Radiol* 2012;47:688-696
21. Rheinheimer S, Stieltjes B, Schneider F, Simon D, Pahernik S, Kauczor HU, et al. Investigation of renal lesions by diffusion-weighted magnetic resonance imaging applying intravoxel incoherent motion-derived parameters--initial experience. *Eur J Radiol* 2012;81:e310-e316
22. Luciani A, Vignaud A, Cavet M, Nhieu JT, Mallat A, Ruel L, et al. Liver cirrhosis: intravoxel incoherent motion MR imaging--pilot study. *Radiology* 2008;249:891-899
23. DeLong ER, DeLong DM, Clarke-Pearson DL. Comparing the areas under two or more correlated receiver operating characteristic curves: a nonparametric approach. *Biometrics* 1988;44:837-845
24. Landis JR, Koch GG. The measurement of observer agreement for categorical data. *Biometrics* 1977;33:159-174
25. Squillaci E, Manenti G, Cova M, Di Roma M, Miano R, Palmieri G, et al. Correlation of diffusion-weighted MR imaging with cellularity of renal tumours. *Anticancer Res* 2004;24:4175-4179
26. Manenti G, Di Roma M, Mancino S, Bartolucci DA, Palmieri G, Mastrangeli R, et al. Malignant renal neoplasms: correlation between ADC values and cellularity in diffusion weighted magnetic resonance imaging at 3 T. *Radiol Med* 2008;113:199-213
27. Zhang JL, Sigmund EE, Chandarana H, Rusinek H, Chen Q, Vivier PH, et al. Variability of renal apparent diffusion coefficients: limitations of the monoexponential model for diffusion quantification. *Radiology* 2010;254:783-792
28. Gaing B, Sigmund EE, Huang WC, Babb JS, Parikh NS, Stoffel D, et al. Subtype differentiation of renal tumors using voxel-based histogram analysis of intravoxel incoherent motion parameters. *Invest Radiol* 2015;50:144-152
29. Inci E, Hocaoglu E, Aydin S, Cimilli T. Diffusion-weighted magnetic resonance imaging in evaluation of primary solid and cystic renal masses using the Bosniak classification. *Eur J Radiol* 2012;81:815-820
30. Goyal A, Sharma R, Bhalla AS, Gamanagatti S, Seth A, Iyer VK, et al. Diffusion-weighted MRI in renal cell carcinoma: a surrogate marker for predicting nuclear grade and histological subtype. *Acta Radiol* 2012;53:349-358
31. Mytsyk Y, Borys Y, Komnatska I, Dutka I, Shatynska-Mytsyk I. Value of the diffusion-weighted MRI in the differential diagnostics of malignant and benign kidney neoplasms - our clinical experience. *Pol J Radiol* 2014;79:290-295
32. Padhani AR, Liu G, Koh DM, Chenevert TL, Thoeny HC, Takahara T, et al. Diffusion-weighted magnetic resonance imaging as a cancer biomarker: consensus and

recommendations. *Neoplasia* 2009;11:102-125
33. Wang H, Cheng L, Zhang X, Wang D, Guo A, Gao Y, et al. Renal cell carcinoma: diffusion-weighted MR imaging for subtype differentiation at 3.0 T. *Radiology* 2010;257:135-143
34. Koh DM, Collins DJ, Orton MR. Intravoxel incoherent motion in body diffusion-weighted MRI: reality and challenges. *AJR Am J Roentgenol* 2011;196:1351-1361
35. Chen X, Qin L, Pan D, Huang Y, Yan L, Wang G, et al. Liver diffusion-weighted MR imaging: reproducibility comparison of ADC measurements obtained with multiple breath-hold, free-breathing, respiratory-triggered, and navigator-triggered techniques. *Radiology* 2014;271:113-125